Molecular Dynamics Simulation Studies of Polyether and Perfluoropolyether Surfactant Based Reverse Micelles in Supercritical Carbon Dioxide

Sanjib Senapati and Max L. Berkowitz*

Department of Chemistry, University of North Carolina at Chapel Hill, Chapel Hill, North Carolina 27599

Received: April 25, 2003; In Final Form: September 8, 2003

Molecular dynamics simulations are performed to investigate the structural properties of aqueous reverse micelles in supercritical carbon dioxide. A carboxylate perfluoropolyether is used as the surfactant in the first simulation. The results show that the micelle remains stable over a 5 ns time period. Calculated micellar properties are found to be in good agreement with the available experimental data. Two other simulations are performed on systems where all fluorine atoms of the surfactant molecules are replaced with hydrogen atoms. In the first of these simulations the number of molecules is the same as in the simulation with perfluorinated surfactant. In the second simulation the exposure of an aqueous core to carbon dioxide is similar to the one observed in the simulation with perfluorinated surfactant. We observe that fluorinated chains coordinate more carbon dioxide molecules compared to the pure polyether chains. This has a direct influence on the micellar structure.

1. Introduction

Supercritical carbon dioxide is often considered as an ideal solvent substitute because it is a nontoxic, chemically inert, cheap, highly volatile, nonflammable, and potentially recyclable fluid. But many important classes of substances, e.g., water, biomolecules, and polymers, exhibit low solubility in supercritical carbon dioxide ($scCO_2$). Recently, several experimental efforts were focused on finding suitable surfactants that are capable of stabilizing microdispersion of aqueous or polymer phases in CO_2. Conventional hydrocarbon surfactants used in oil/water systems are shown to exhibit low solubilities in carbon dioxide, and therefore, are not capable of solubilizing a significant amount of water.[1] Surfactants with perfluorinated chains, on the other hand, are quite soluble in $scCO_2$.[2−7] Thus, Johnston and co-workers[2] reported the microemulsion formation of water-in-CO_2 (W/C) using a hybrid dichain sulfate surfactant. In addition, they demonstrated that perfluoropolyether-based microemulsions also produce a thermodynamically stable aqueous domain in a CO_2 phase.[3] DeSimone and co-workers[4] have developed surfactants with CO_2-philic perfluorooctylacrylate tails that form microemulsions in $scCO_2$. Very recently, they have reported that microemulsions based on dichain phosphate fluorosurfactants also allow for significant water uptake through the formation of W/C microemulsions.[5] Eastoe and co-workers[6] reported anionic phosphate fluorosurfactants capable of W/C microemulsion formation. All the surfactants mentioned above, when placed in $scCO_2$ are shown to form reverse micelles (RM), and therefore are promising materials for extending W/C microemulsions to a variety of applications, e.g., in selective extraction of polar compounds from aqueous solution, in emulsion polymerization schemes, or as a media for reactions between polar and nonpolar molecules.

Small-angle neutron scattering (SANS) experiments on W/C microemulsions were recently performed over a large range of pressure, temperature, and droplet volume fraction.[5,6,8−13] These studies revealed the existence of spherical water droplets of radius 20−35 Å dispersed in CO_2. Various spectroscopic techniques, e.g., Fourier transform infrared (FTIR), UV−vis, fluorescence, and electron paramagnetic resonance experiments, demonstrated the existence of a bulk water domain in these systems.[3,14] Small-angle X-ray scattering experiments[15,16] were used to confirm directly the formation of nanometer-sized microemulsions and to develop a model of colloidal shape and structure.

Although useful information about the structure of reverse micelles in microemulsions can be obtained from experiments, computer simulation methods can play a major role in developing our understanding of W/C microemulsions in a more detailed manner and in interpreting experimental observations.[13,17−19] Very recently, we reported the structure of a reverse micellar aggregate composed of a dichain phosphate fluorosurfactant in W/C microemulsion. By combining data from molecular dynamics simulation and SANS experiments, we have estimated the size and shape of the reverse micelle.[13] In a followup publication, we, using molecular dynamics simulations observed the presence of a bulk water domain in the aggregated core of RM and demonstrated how the structure and dynamics of interfacial water are affected due to the presence of surfactant headgroups.[17] An encouraging match between simulation results and experimental data was observed in these studies. Research on W/C microemulsions using computer simulation techniques has also being carried out by Cummings and co-workers.[18,19] They performed a molecular dynamics simulation on a system of water/dichain surfactant/$scCO_2$ and demonstrated the self-assembly of reverse micelles in this system.[18] They also studied the structural properties and the kinetics of aggregation of such micelles.[19] A good agreement with the available experimental data was attained in their calculations.

The commercially available perfluoropolyether ammonium carboxylate surfactant, $CF_3-(O-CF_2-CF(CF_3))_3-O-CF_2-COO^-NH_4^+$ ($PFPECOO^-NH_4^+$), $M_w = 695.13$, has been shown to form aqueous RM in supercritical CO_2 with water to surfactant mole ratios (W_o) up to 30.[3,12] In this work, we use

10.1021/jp035128s CCC: $25.00
Published on Web 10/31/2003

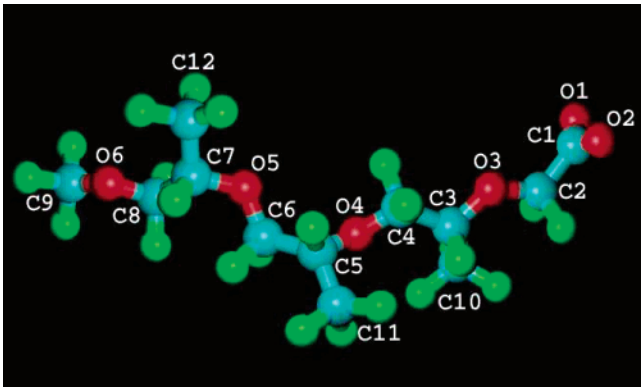

Figure 1. Structure of the surfactant anion PFPECOO$^-$. Color scheme: red balls, oxygens; cyan balls, carbon atoms; green balls, fluorine atoms.

the molecular dynamics simulation technique to investigate the structural properties of the aqueous RM containing PFPECOO$^-$NH$_4^+$ surfactant in scCO$_2$ with a W_o value of 8.4. Our simulation results show very good agreement with experimental data and offer detailed information on the shape and structure of the system.

One particular issue we want to focus on is the importance of fluorine atoms in the packing of PFPE tails and related properties, e.g., tail solvation. To understand this issue deeper, we carry out a series of other simulations where we study a model surfactnat, polyether ammonium carboxylate, which is analogous to PFPECOO$^-$NH$_4^+$ except that all fluorine atoms are replaced by hydrogen atoms in W/C system.

2. The Model and Simulation Details

We performed a number of molecular dynamics (MD) simulations on systems containing aqueous reverse micelles in supercritical carbon dioxide. The fluorinated polyether PFPECOO$^-$NH$_4^+$ was used as the surfactant in the primary simulation, whereas its nonfluorinated analogue CH$_3$−(O−CH$_2$−CH(CH$_3$))$_3$−O−CH$_2$−COO$^-$NH$_4^+$ (PECOO$^-$NH$_4^+$) was used in the other simulations. The SPC/E model[20] was chosen to describe the water molecules. The SPC/E model is a well-tested and widely used model for liquid water, which has been shown to give a good description of liquid water at both room and supercritical conditions. We follow an all-atom approach to model the anionic parts PFPECOO$^-$ and PECOO$^-$ of the surfactants. A picture of the surfactant anion PFPECOO$^-$ is presented in Figure 1. The consistent valence force field[21−23] (CVFF) parameters were used to describe the intermolecular and intramolecular interactions present in the surfactant anions. The CVFF force field has been successfully applied to study the rheological behavior of confined branched and linear perfluropolyethers and hydrocarboxylic acids.[23] Very recently, Rossky and co-workers have applied the same force field for PFPECOO$^-$ anion at the water/CO$_2$ planar interface.[24] To calculate the values of the point charges, we used Accelrys' Material Studio software[22] with the CVFF force field. The corresponding potential parameters and also the point charges for the surfactants can be found in Table 1. The OPLS set of intermolecular parameters has been used to model NH$_4^+$ counterions. These parameters are shown to reproduce the experimental heat of solution and hydration number of ammonium ion in water.[25] The five-site model of ammonium ion consists of one Lennard-Jones (LJ) site on the central *N* atom and five sites for point charges. The rigid EPM2 model[26] proposed by Harris and Yung is used to describe CO$_2$. This model accurately reproduces the experimental critical point and liquid−vapor coexistence curve and is being widely used. It is a three-site model with each site represented by a Lennard-Jones sphere with an embedded central point charge. The rigid EPM2 model has a linear geometry with the C−O bond length of 1.149 Å. The intermolecular potential parameters along with the site charges are also included in Table 1.

TABLE 1: Force Field Parameters for the Various Species Present in the Systems[a]

(a) Partial Charges

atom type	charge (*e*)	atom type	charge (*e*)	atom type	charge (*e*)
For H$_2$O, CO$_2$ and NH$_4^+$ Cation					
O$_w$	−0.8476	C$_c$	0.6512	N$_a$	−0.4000
H$_w$	0.4238	O$_c$	−0.3256	H$_a$	0.3500
For PFPECOO$^-$ Anion					
O1, O2	−0.570	O3, O4, O5, O6	−0.300	C9	0.975
C1	0.140	C3, C5, C7	0.425	C10, C11, C12	0.825
C2	0.700	C4, C6, C8	0.700	F	−0.275
For PECOO$^-$ Anion					
O1, O2	−0.570	O3, O4, O5, O6	−0.300	C9	−0.150
C1	0.140	C3, C5, C7	0.050	C10, C11, C12	−0.300
C2	−0.050	C4, C6, C8	−0.050	H	0.100

(b) Bond Parameters

bond	k_b [kJ/(mol Å^2)]	r_o (Å)	bond	k_b [kJ/(mol.Å^2)]	r_o (Å)
O$_w$−H$_w$		1.000	C−C	1351.1465	1.526
C$_c$−O$_c$		1.149	C−O	1143.8338	1.425
N$_a$−H$_a$		1.010	C−F	2076.6528	1.363
C$^-$−O$^-$	2260.8720	1.250	C−H	1426.1000	1.105
C$^-$−C	1185.2513	1.520			

(c) Angle Parameters

angle	k_θ [kJ/(mol rad^2)]	θ_o (deg)	angle	k_θ [kJ/(mol rad^2)]	θ_o (deg)
O$_w$−H$_w$−O$_w$		109.50	O−C−C	293.0760	109.50
H$_a$−N$_a$−H$_a$	146.4400	109.47	C−C−C	195.1049	110.50
O$^-$−C$^-$−O$^-$	607.0860	123.00	F−C−C	414.4932	107.80
O$^-$−C$^-$−C	284.7024	120.00	F−C−F	397.7460	107.80
C$^-$−C−O	293.0760	109.50	C$^-$−C−H	188.4060	109.50
C$^-$−C−F	414.4932	107.80	H−C−O	238.6477	109.50
F−C−O	397.7460	107.80	H−C−C	185.8940	110.00
C−O−C	251.2080	109.50	H−C−H	165.3790	106.40

(d) Dihedral Parameters

dihedral	A [kJ/(mol rad)]	ϕ_o	m
−C$^-$−C−	0.0000	0.0	0
−C−O−	1.6328	0.0	3
−C−C−	5.9557	0.0	3

(e) Improper Dihedral Parameters

dihedral	B [kJ/(mol.rad)]	χ_o	n
O$^-$−O$^-$−C$^-$−C	48.5669	180.0	2

(f) van der Waals Parameters

atom type	σ_{ii} (Å)	ϵ_{ii} (kJ/mol)	atom type	σ_{ii} (Å)	ϵ_{ii} (kJ/mol)
O$_w$	3.165	0.650	O$^-$	2.860	0.955
H$_w$	0.000	0.000	C$^-$	3.617	0.620
C$_c$	2.757	0.234	C	3.474	0.670
O$_c$	3.033	0.669	O	2.860	0.955
N$_a$	3.250	0.712	F	3.081	0.288
H$_a$	0.000	0.000	H	2.449	0.159

[a] w stands for water, c stands for CO$_2$, and a stands for NH$_4^+$ cation. C$^-$ stands for carboxylate carbon, O$^-$ stands for carboxylate oxygen, C stands for alkyl carbon, O stands for ether oxygen, and H stands for surfactant hydrogen.

The total potential energy of the system can be expressed as

$$U = U_{\text{inter}} + U_{\text{intra}} \tag{1}$$

where U_{inter} and U_{intra} are the energies due to intermolecular and intramolecular interactions, respectively. The intermolecular interaction potential between ith and jth particle is described as a sum of the LJ potential and Coulomb interactions of partial charges,

$$U_{\text{inter}} = \sum_i \sum_{j>i} 4\epsilon_{ij}[(\sigma_{ij}/r_{ij})^{12} - (\sigma_{ij}/r_{ij})^{6}] + q_i q_j / r_{ij} \tag{2}$$

The cross interactions (i.e., LJ terms) are obtained by using the Lorentz−Berthelot combining rule except that for CO_2. For CO_2 the cross interaction terms are obtained by using the geometric mean as required by the EPM2 model,

$$\epsilon_{\text{co}} = \sqrt{\epsilon_{\text{c}}\epsilon_{\text{o}}} \qquad \text{and} \qquad \sigma_{\text{co}} = \sqrt{\sigma_{\text{c}}\sigma_{\text{o}}} \tag{3}$$

The intramolecular potential for the surfactant anions is described in the following form:

$$U_{\text{intra;anion}} = \sum_i k_{\text{b}}(r_i - r_{\text{o}})^2 + \sum_i k_\theta(\theta_i - \theta_{\text{o}})^2 + \sum_i A[1 + \cos(m\phi_i - \phi_{\text{o}})] + \sum_i B[1 + \cos(n\chi_i - \chi_{\text{o}})] \tag{4}$$

where the terms represent the harmonic bond stretching potential, angle bending potential, dihedral potential, and improper dihedral potential, respectively. Here, k_{b} is the bond force constant, which is a measure of the rigidity of the bond, r_{o} is the equlibrium bond length, k_θ is the angle bending force constant, θ_{o} is the equlibrium angle, A is the dihedral force constant, m is the periodicity, ϕ_i is the dihedral angle defined as the angle between the normal to the two planes, each of which is formed by three successive interaction sites, and χ_i is the improper dihedral angle. For CVFF, the model parameters are optimized on the basis of full 1−4 vdw and electrostatic interactions. All bond lengths in water and ammoniun counterions are held fixed by applying the SHAKE algorithm[27] with a preset tolerance of 10^{-8} Å. For rigid CO_2, we employ Fincham's implicit quaternion formulation[28] of the equations of rotational motion and for the integration over time, we adapt the standard leapfrog algorithm with a time step of 2 fs.

The primary system (system 1) we simulated contained 554 water molecules, 66 fluorinated surfactant molecules, and 6359 CO_2 molecules placed in a cubic box at 25 °C and 200 bar pressure. Thus, the system contained a total of 23 775 particles. The values for the temperature, pressure, and W_{o} are the same as the values present in the NMR studies of water transport in W/C microemulsions by Johnston and co-workers.[29] The number of surfactant and water molecules were obtained by using the following formulas for the area of the aqueous core (A_{c}) and from the experimental values for the area per headgroup ($A_{\text{h}} = 76$ Å^2), radius of the aqueous core ($R_{\text{c}} = 20$ Å), and $W_{\text{o}} = 8.4$,

$$A_{\text{c}} = 4\pi R_{\text{c}}^{\,2} = A_{\text{h}} N_{\text{h}} \qquad W_{\text{o}} = N_{\text{w}}/N_{\text{h}} \tag{5}$$

where N_{h} and N_{w} are the number of surfactant headgroups and water molecules, respectively. A large number of CO_2 molecules was taken to attain a bulk CO_2 phase and to discard any possibility of interdroplet (interaggregate) interactions due to the application of periodic boundary condition.

Our simulation was started from a configuration represented by an aggregate in which we distributed the surfactant molecules around the periphery of a sphere of radius 16 Å. Surfactant molecules pointed their headgroups inward and their tails outward in the initial configuration. The sphere of radius 16 Å was chosen on the basis of the fact that 554 water molecules can be accommodated in that volume. Extensive equilibration and thermalization of this highly ordered structure was performed, keeping the carboxylate carbon atoms fixed to remove the initial strain. After that, we added water molecules and NH_4^+ ions to the empty space inside the sphere and performed another set of minimization and thermalization runs, this time letting the carboxylate carbon atoms go free. The obtained structure was then inserted into the hole made in the middle of a cubic box containing CO_2 molecules at the density of 0.95 g/mL. The value for the density of CO_2 in the box was taken to be slightly higher than the desired value of 0.92 g/mL corresponding to the experimental density. This was done on purpose, because we expected that some carbon dioxide molecules will diffuse into the intertail region of the micelle and therefore will bring down the bulk density of CO_2 to a value somewhat closer to the desired value. The final set of minimization and thermalization runs was performed before a 500 ps equilibration run. To enable the volume variation, the equilibrations and production runs were perfomed in NPT ensemble, using the Nose−Hoover thermostat and barostat.[30] Both the thermostat and barostat relaxation times were set to 0.5 ps.

This configuration obtained at the end of 500 ps run provided the initial configuration for the production run of 5 ns. Periodic boundary conditions were employed in all directions. The calculation of the long-range Coulombic forces was performed using the smooth particle mesh Ewald (SPME) method.[31] The real space part of the Ewald sum and Lennard-Jones interactions were cut off at 10 Å.

The other systems we simulated contained 66 nonfluorinated surfactant molecules, 6359 CO_2 molecules, and a varying number of water molecules at 25 °C and 200 bar pressure. The first system in this series (system 2) contained 554 water molecules, i.e., the same amount of water as was present in the fluorinated surfactant system. The simulation for this system was also started from an aggregated configuration. A 500 ps equilibration run was then performed before a production run of 5 ns in NPT ensemble. The other simulation details are exactly the same as that in system 1. The subsequent systems contained a reduced number of water molecules. The starting configurations for these systems were obtained from the final configuration of system 2 (i.e., at 5 ns) but with a smaller number of water molecules. In other words, a different amount of water molecules was taken out separately from the final configuration of system 2 to generate the starting configurations for a number of systems of different water content. Each of these systems was simulated for a few nanoseconds. The final system we analyzed contained 200 water molecules (system 3). The reason for choosing this system will be discussed in the next section. System 3 was also simulated for a production run of 5 ns.

All the simulations were carried out using the DLPOLY[32] molecular dynamics simulation package.

3. Results and Discussion

3.1. Fluorinated Surfactant System. In this subsection, we present the results obtained from the simulation on our primary system consisting of fluorinated surfactants. Varieties of experiments[11,29] were already performed to explore the properties of this system and we have compared our simulation results with the experimental data wherever available. We also present a

detailed molecular description of the system that is very difficult, even sometimes impossible, to obtain by means of experimental techniques.

3.1.1. Micelle Size. The general structural properties of a reverse micelle can be characterized by the size and shape of its aqueous core. A useful statistical measure of the size of a micelle is its radius of gyration, R_g. We calculate R_g for the aqueous core by using the following formula,

$$R_g^2 = \sum_i m_i(r_i - r_o)^2 / \sum_i m_i \qquad (6)$$

where i includes water molecules in the core, NH_4^+ counterions, the carboxylate group, the adjacent CF_2 group and the first ether oxygen (O3) in each of the surfactant tails. The reason for including the first CF_2 group and the first ether oxygen in the calculation is given below. Here, m_i is the mass and r_i is the distance of atom i from the center of mass r_o of the aggregated core. The radius of gyration of a spherical aggregate with uniform mass distributions is related to its radius R_c by a simple relation: $R_g^2 = (3/5)R_c^2$. Although, the uniform mass assumption does not hold in our case, this relationship, which is also used by the experimentalists, can provide us with an estimate of the core radii of the RM.

The CF_2 group (C2) and the ether oxygen (O3) of the surfactant tails are included in the calculation of the gyration radius because they are found to be well solvated in water. This can be seen from the pair radial distribution functions (rdf) of water oxygen (O_w) with the central atom of various groups present in the surfactant tail. In Figure 2, we have plotted the rdfs for the pairs of O_w-C1, O_w-C2, O_w-O3, O_w-C3, and O_w-C4 (for the atom notation see Figure 1). The figure clearly shows that water penetrates the headgroups region and solvates the carboxylate group, first CF_2 group, and first ether oxygen group of the surfactant tail. Water density then gradually diminishes and any group beyond O3 does not contribute much to the calculation of R_g.

The time history of the core radius of the RM during the entire 5 ns of the production run is presented in Figure 3. We observe that the aggregated core is stable, because the figure indicates that the average value of R_c is stable in time. This average value is 19.2 ± 0.5 Å, which is in very good agreement with the experimental value of 20 Å obtained for the aqueous droplet in $PFPECOO^-NH_4^+$/water/carbon dioxide system.[29]

3.1.2. Micelle Shape. The stability of the aggregate can be further tested by examining the time evolution of its eccentricity e. Eccentricity of the aggregate can also provide us with a quantitative measure of the micellar shape. We define the micelle eccentricity as

$$e = 1 - \frac{I_{min}}{I_{avg}} \qquad (7)$$

where I_{min} is the moment of inertia of the micelle along the x, y, or z axis with the smallest magnitude and I_{avg} is the average of all three moments of inertia. The time evolution of the eccentricity during the 5 ns run is plotted in Figure 4. The eccentricity for the fluorinated surfactant system is found to fluctuate around the average value of 0.05. For a perfect sphere, the eccentricity should be zero. The value of e in our primary system indicates that the aggregate is essentially spherical. We also confirm our previous observation that the micelle is stable in time, because the value of the eccentricity is rather stable. For a visual inspection of the micellar shape, we present the snapshots of the micellar aggregate at two different times, 3.47 and 4.49 ns. These are times when the corresponding aggregates have maximum and minimum values of eccentricity, respectively. These times are denoted by circles in Figure 4, and the corresponding snapshots of the micelle are presented in Figure 5. In both the snapshots, the solvent molecules are intentionally hidden to see the micellar aggregate clearly. As we can see from these pictures, our micelle is essentially spherical, although the shape of the micelle in Figure 5a is somewhat less spherical as the value of its eccentricity would predict.

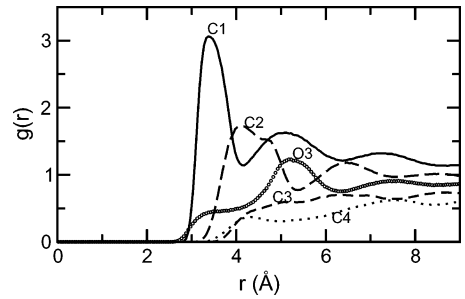

Figure 2. Radial distribution functions between water oxygen and various atoms along the $PFPECOO^-NH_4^+$ surfactant backbone. Atom notations are the same as shown in Figure 1.

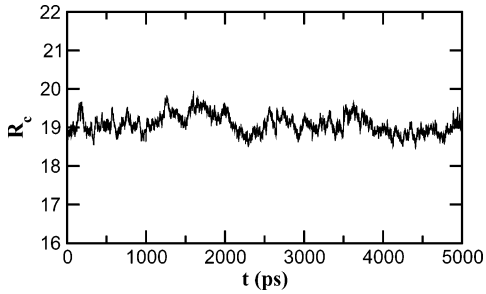

Figure 3. Time history of the core radius during the 5 ns production run for the fluorinated surfactant system.

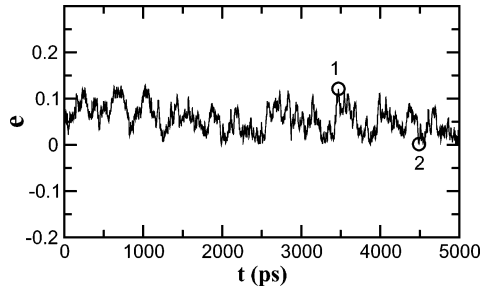

Figure 4. Time evolution of the eccentricity for the fluorinated surfactant system. Circles 1 and 2 correspond to the times at which the eccentricity is maximum and minimum.

The observed fluctuations in the size or shape of the micelles are dictated not only by the temperature but also by interfacial tensions in the systems. These depend on the model potentials, and it will be interesting to study how models of different sophistication influence the fluctuation character of the micelles.

3.1.3 Accessible Surface Area per Headgroup. Another important structural quantity we can calculate is the surface area per headgroup available for the interaction with water. This can be calculated in a number of ways. In one approach we follow the method of Lee and Richards[33] to determine this quantity. According to this method, we remove all the water molecules and NH_4^+ counterions from the aqueous core in the micelle and roll a probe across the entire inner surface formed by the headgroups. The total contact area is then divided by the number of surfactant molecules to obtain the average area per headgroup. A probe of size 1.4 Å is utilized to mimic the size of the water

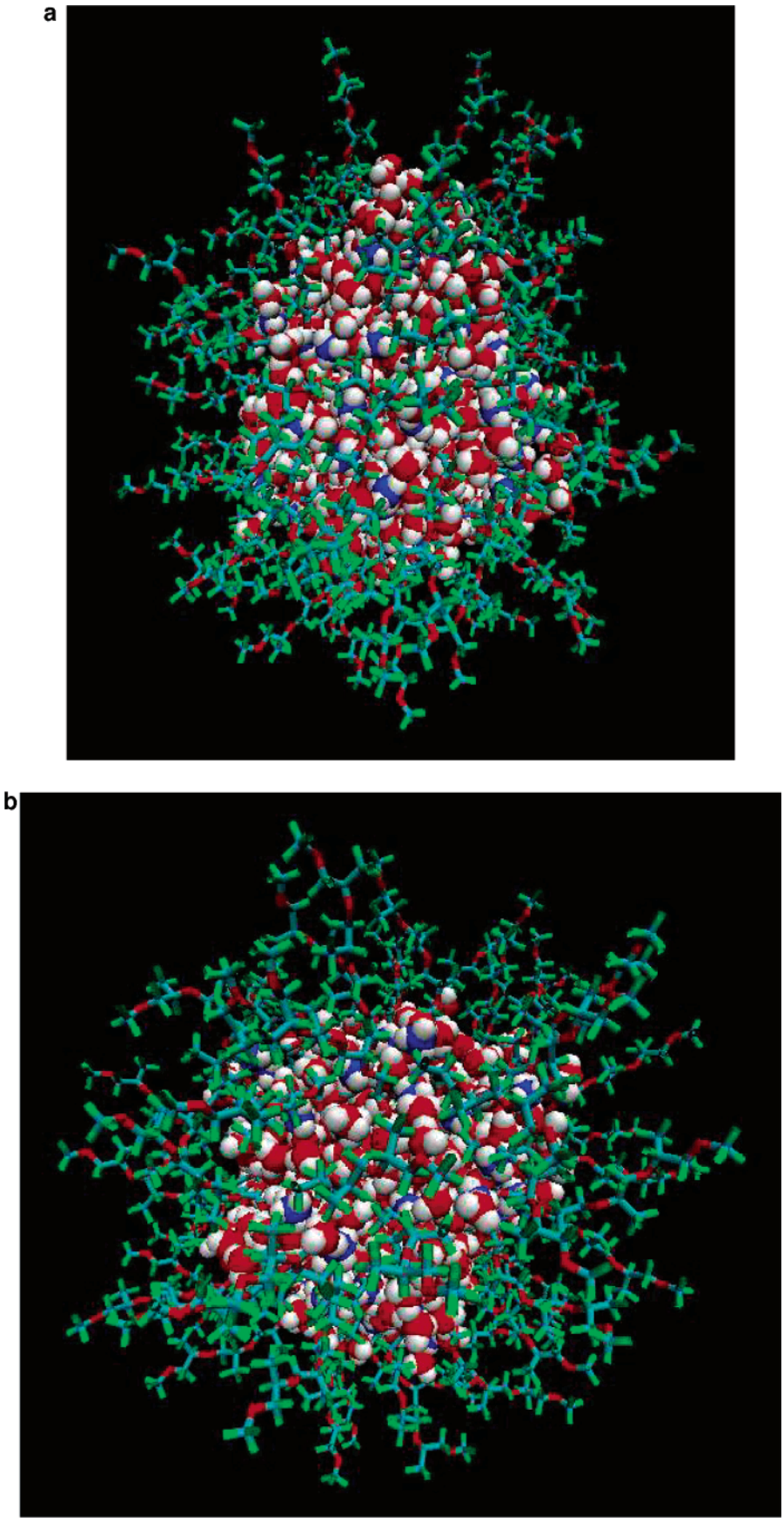

Figure 5. Snapshots of the fluorinated micelle at two different times: (a) at 3.47 ns and (b) at 4.49 ns. These are the times when the micellar aggregate displays the maximum and the minimum values of the eccentricity, respectively. The solvent molecules are omitted for clarity. Color scheme: red balls, water oxygens; white balls, either water or ammonium hydrogens; blue balls, nitrogens of the ammonium cation. The surfactant anions are represented by sticks: red sticks, oxygens; cyan, carbon atoms; green sticks, fluorine atoms in the surfactant chains.

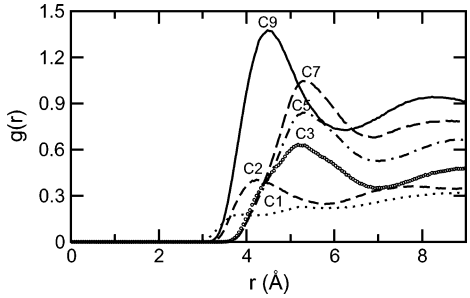

Figure 6. Radial distribution functions between carbon dioxide carbon and the various C atoms along the fluorinated surfactant backbone. Atom notations are the same as shown in Figure 1.

molecule. By performing this procedure, we obtained the area per headgroup, $A_h = 63.3 \pm 6$ Å^2 for $PFPECOO^-NH_4^+$ surfactant.

One can also estimate the area per headgroup by using the equation connecting the surface area of the aqueous core (A_c) and the calculated value of the radius of the aqueous core (R_c),

$$A_c = 4\pi R_c^2 = A_h N_h \tag{8}$$

where N_h is the number of surfactant molecules. Using the calculated value of $R_c = 19.2$ Å and $N_h = 66$, we get $A_h = 70.2$ Å^2. This value of surface area is consistent with the value obtained by using the method of Lee and Richards. The corresponding value of the area estimated from the experiment is 76 Å^2.[11,29]

3.1.4. Solvation of Hydrophobic Tails in CO_2. Experimental studies indicate that surfactants with fluoroalkyl or fluoroether tails exhibit high solubility in $scCO_2$. An insight into the structure of CO_2 around the surfactant tails can be provided by the radial distribution functions (rdf). We display the rdfs between the carbon atom (C_c) of CO_2 and various carbon atoms along the fluorosurfactant backbone in Figure 6. The existence of pronounced peaks in g_{Cc-C9}, g_{Cc-C7}, g_{Cc-C5}, and g_{Cc-C3} (for atom notations see Figure 1) implies that the fluoro surfactant tails are well solvated in CO_2. Carbon dioxide is seen to penetrate the tail region even further and solvate the first CF_2 group (C2) also. However, C2 is found to be 15% less solvated than C9 or C3 in CO_2. This is due to the fact that water penetrates the headgroup region and solvates C2. It is the competition between water and CO_2 that results in a smaller exposure of C2 to CO_2. The CO_2 density diminishes around the carboxylate carbon (C1), which is seen to be solvated in water.

We have determined the average solvation number of the surfactants by counting the number of CO_2 molecules in the first solvation shell of the surfactants. We noticed a substantial overlap between the solvation shells of two adjacent atoms in the same chain (intrachain). A substantial overlap is also seen between the solvation shells of atoms in the adjacent chains (interchain). The latter is particularly true for those atoms that are closer to headgroups, because the curvature is larger in this region. Therefore, while calculating the solvation number, we counted each CO_2 molecule in the tail region just once. The average value of the solvation number we got for the fluorinated surfactant is 15.

3.1.5. Aqueous Core Exposure. A molecular graphics analysis shows that the interior aqueous core is somewhat exposed to CO_2. A similar core exposure was also seen by Tobias and Klein[36] in a MD simulation of calcium carbonate/calcium sulfonate reverse micelle. To get a quantitative estimate of the core exposure, we calculated the core surface area exposed to CO_2 by using the method of Lee and Richards.[33] Following this method, we removed all of the CO_2 molecules from the system and rolled a probe across the surface of the micelle. The contributions to accessible area from water and ammonium counterions were summed to estimate the core exposure. For comparison, the area of a bare aqueous core was also calculated by removing the surfactant molecules from the system. A 2.0 Å probe was utilized to mimic the CO_2 molecules in the system. We observed that the average value of the accessible surface area for bare aqueous core is 6988 ± 200 Å^2. This should be compared with the area of 838 ± 170 Å^2 when the surfactants are present in the system. These values show that about 12% of the aqueous core is exposed to CO_2.

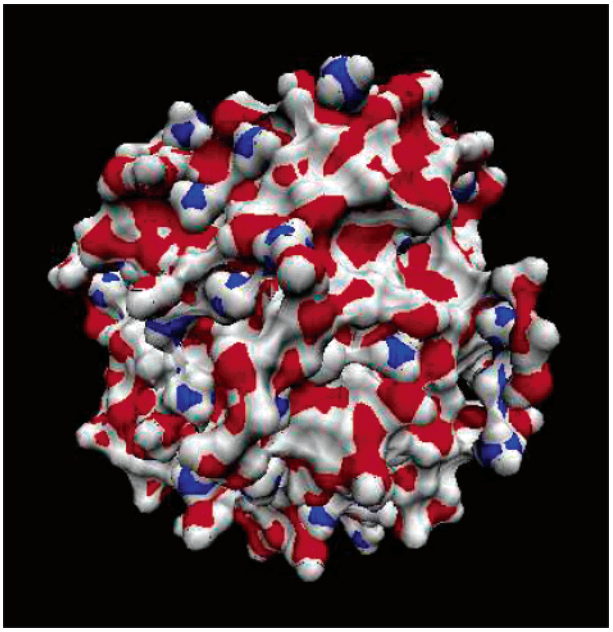

Figure 7. Snapshot of the bare aqueous core for the fluorinated surfactant system at 5 ns. Color scheme: red, water oxygens; white, either water or ammonium hydrogens; blue, nitrogens of ammonium cation.

We also noticed that the calculated value of the surface area for bare aqueous core is higher than the value that can be computed using the expression that contains R_c. This is due to the fact that the micellar core is not spherical; rather it has a corrugated and rough surface. In Figure 7, we have presented a picture of the bare core for the fluorinated system at 5 ns. This picture clearly demonstrates that the surface of the bare core is very rough and corrugated.

3.1.6. Tail Conformations. To understand more fully the properties of the reverse micelle in our system, we also examined the conformational properties of the surfactant tails. In Figure 8 we have plotted the average fraction of gauche defects for each dihedral angle present in the fluorinated surfactant anions. The dihedral angles are numbered beginning with the O1−C1−C2−O3 (carboxylic and the CF_2 carbon as the central atoms) fragment and ending with the C7−C8−O6−C9 fragment. The angle is considered to be trans if it falls into the range 120−240°, the remainder being gauche. The figure shows that the dihedral angles 4, 5, 7, 8, 10, and 11 prefer to be trans. Most of the other dihedrals in the case of fluorinated surfactants favor a gauche conformation. A similar distribution was obtained by da Rocha et al. in a simulation of the $PFPECOO^-$ surfactant at water/CO_2 planar interface.[24] da Rocha et al. explained the result as due to a balance between steric crowding emanating from the presence of large F atoms, the

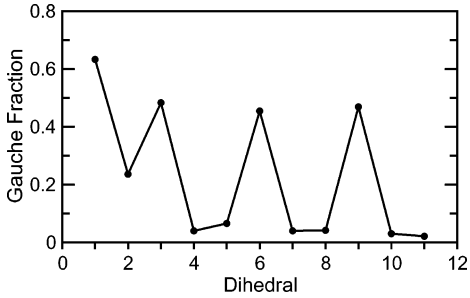

Figure 8. Average fraction of gauche defects for each dihedral angle present in the fluorinated surfactant. The dihedral angles are numbered beginning with the O1−C1−C2−O3 fragment and ending with the C7−C8−O6−C9 fragment. Atom notations are the same as shown in Figure 1.

presence of the pendant CF_3 groups, and flexibilty due to the ether linkages to the fluorinated chain.[24]

3.1.7. Aggregate Microstructure. After establishing the validity of our models by finding that a good agreement exists between our results and the experimental data, we further explore various microscopic properties of the system. To get an idea about the average structure of the micelle, we present a snapshot picture of a cross section of the system at 5 ns, which is shown in Figure 9. This figure shows that the aggregated core is essentially spherical, in accordance with our previous calculations. The aqueous phase is trapped in the middle of the aggregate with the surfactant molecules surrounding it. The carboxylate headgroups are distributed at the surface of the aqueous core. The observed distribution of ammonium counterions indicates the possibility of ion-pair formation between NH_4^+ and the carboxylate headgroups. The tails of the surfactants are extending out and are solvated in CO_2. CO_2 molecules penetrate the tail region but are still present in excess to offer a bulk phase.

The microscopic structure of the micelle can be characterized by atomic radial densities of various species present in the system. Figure 10 shows the density of constituents in the fluorinated system measured as a function of the distance from the center of the aqueous core. The number densities are calculated by computing the average number of molecules in spherical shells of thickness $\delta r = 0.2$ Å, located at various distances from the center of the water pool. The first few points in the plot are discarded due to bad statistics. These points correspond to the first few spherical shells that have very small volumes. The figure indicates the existence of an aqueous core region, the interface region between the water core and the headgroups, and another interface region between the tails and carbon dioxide. As we can see, the interfacial regions are rather wide, and this is consistent with other observations made in other simulations on reverse micellar systems.[13,19] Figure 10 also shows that the ammonium counterions and the carboxylate headgroups are solvated in water. We also observe that a significant amount of water penetrates the hydrophobic region and essentially hydrates the CF_2 group (C2) that is adjacent to

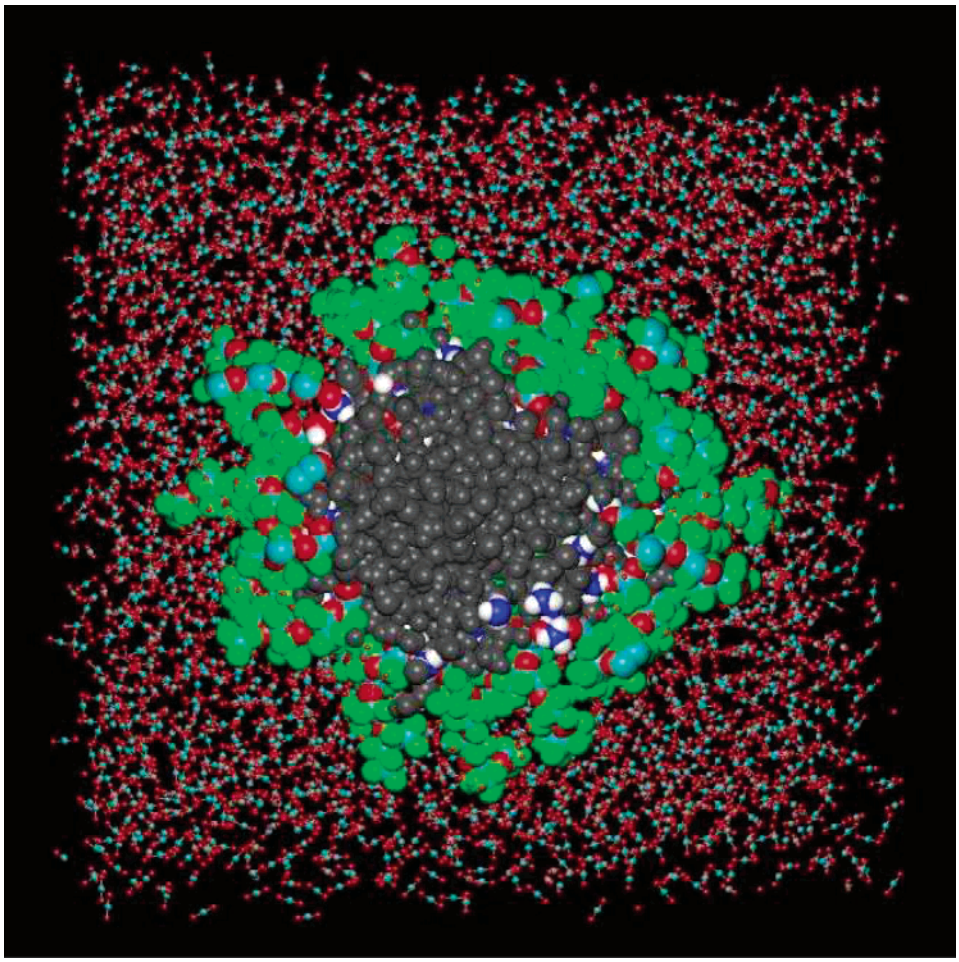

Figure 9. Snapshot of the cross section of the fluorinated system at 5 ns. Color scheme: red balls, surfactant oxygens; cyan balls, surfactant carbons; green balls, fluorine atoms in the surfactant tails; blue and white balls, nitrogen and hydrogen atoms in ammonium cations; gray balls, water molecules. The atoms of solvent molecules are represented by smaller circles with cyan and red color representing the carbon and oxygen atoms in CO_2.

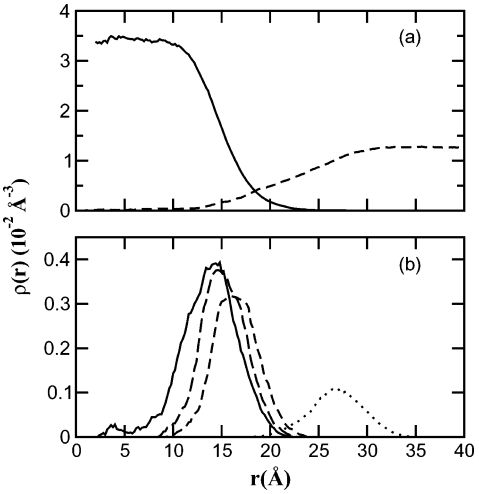

Figure 10. Number density profiles of (a) water (solid line) and carbon dioxide (dashed line) and (b) ammonium counterion (solid line), carboxylate headgroup (long dashed line), tail C2 (short dashed), and tail C9 (dotted line) as a function of the distance from the center of the aqueous core for the fluorinated system. Atom notations are the same as shown in Figure 1.

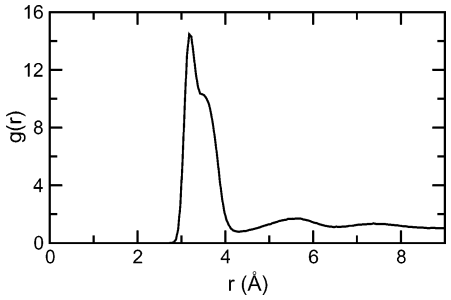

Figure 11. Radial distribution function for ammonium nitrogen−carboxylate carbon pair.

the headgroup. The water density then decays to zero and CO_2 molecules take over in the solvation of the surfactant tails. We found in our simulations that the water density at distances far from the interface is 1.00 g/mL, the same density as found for the bulk SPC/E water at 25 °C and 200 bar pressure. Therefore, it is possible that a bulklike aqueous phase is present in our system. This supports the experimental observation that a bulk water domain exists in the W/C microemulsion systems.[3,14] To understand how close the water inside the reverse micelle is to being bulklike, one needs to study the structure and dynamics of water more carefully. Such a study of water in confined and in micellar environments has been the subject of recent work[17,37−45] and we also plan to perform a more detailed study of water in our system.[46]

A bulk phase is also present in the supercritical CO_2 with a density calculated to be 0.93 g/mL at distances far from the interface. This value is very close to the experimental value of 0.92 g/mL at the specified temperature and pressure. The very good agreement between the bulk values of solvent densities in simulations and experiments indicates that the systems are well equilibrated and the simulation procedures are correct.

For a better understanding of the distribution of ammonium counterions in the reverse micelles, we computed the N−C1 (ammonium nitrogen−carboxylate carbon) pair radial distribution function and calculated the associated coordination number. This rdf is presented in Figure 11. The first peak of the N−C1 rdf reaches its maximum at a distance of 3.2 Å. A small shoulder on the right side of the peak is also observed. The appearance of this shoulder is probably due to the formation of a stable

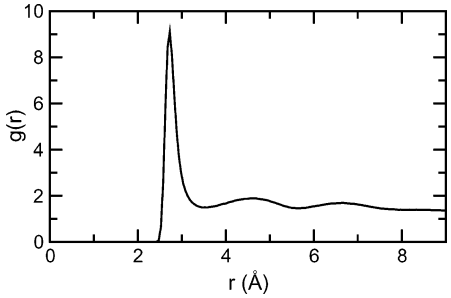

Figure 12. Radial distribution function for ammonium nitrogen−water oxygen pair.

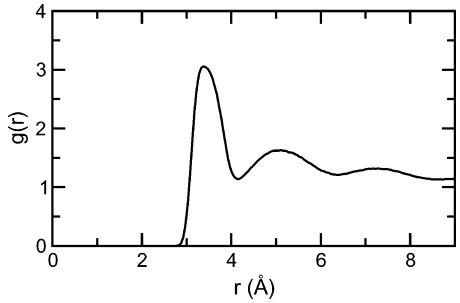

Figure 13. Radial distribution function for carboxylate carbon−water oxygen pair.

site for NH_4^+ ion by a pair of carboxylate oxygens. We found that, on average, 89% of the ammonium ions are within the first shell of the headgroup surface, thus confirming the presence of contact ion pairs in our system. The remaining ions are located in the region of the second peak in the rdf forming solvent-separated ion pairs. Some of the ions are found beyond the second peak, therefore completely dissociating from the surface. These results are consistent with the observations made in other simulations on reverse micelles.[13,19] We noticed that the average percentage of ammonium ions in the first shell varies between 88% and 90% during the production run, thus providing another indication that our simulated systems are quite stable. The average ion coordination number is calculated to be 1.7, indicating that there is a substantial overlap of the C1 coorination shells (ammonium bridging). We also observe from Figure 10 that counterions and headgroups are hydrated in water. Further insight into the structure of water around them can be provided by the respective rdfs. The rdf for the N−O_w (ammonium nitrogen−water oxygen) pair is shown in Figure 12. It shows a distinct hydration shell with a maximum at 2.75 Å due to hydrogen bonding between NH_4^+ and water molecules.[25] The location of the first maximum agrees with the one obtained previously in the study of the dilute aqueous solution of ammonium ion[25] and also with those obtained from the study of ammonium carboxylate surfactant at water/CO_2 interface.[24] The coordination number of the first solvation shell is calculated to be 3.7. This should be compared to the value of 5.7 at infinite dilution. A large reduction in the coordination number confirms the presence of contact ion pairs between the carboxylate headgroup and ammonium counterions in our systems. The second and third shells of water around ammonium ion are more diffused, as indicated by the progressively broader bands.

The rdf for the C1−O_w (carboxylate carbon−water oxygen) pair is shown in Figure 13. The sharp first peak in the rdf is a consequence of the presence of hydrogen-bonded water molecules.[46] The location and the sharpness of the first peak are very similar to the results obtained in the simulations of $HCOO^-$ and CH_3COO^- ions in water.[25] The C1−O_w rdf also shows a distinct separation of the first and second hydration shells, as

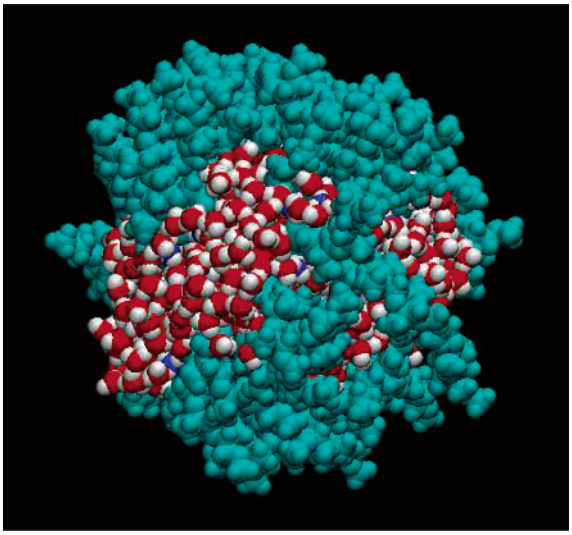

Figure 14. Exposure of the interior aqueous core in system 2. Color scheme: red balls, water oxygens; white balls, either water or ammonium hydrogens; blue balls, nitrogens of ammonium cation; cyan balls, surfactant molecules. The solvent molecules are omitted for clarity.

was observed for the CH_3COO^- ion in water.[25] Integration of the first peak up to the first minimum at 4.1 Å reveals the presence of 4.0 water molecules per carboxylate group. This value is less than the values of 7.3 and 6.6 obtained from simulations of bare formate and acetate ions in water. This reduction in the number of water molecules can be explained by the presence of ammonium counterions in our systems, which, by forming ion pairs with the headgroups, hinder the approach of water molecules to carboxylate groups. da Rocha et al.[24] found that 5 water molecules per carboxylate group are present in their simulation of ammonium carboxylate surfactant at water/CO_2 planar interface. Our value is somewhat smaller than theirs, presumably due to the concave geometry of the headgroup surface and also due to a smaller area per headgroup.

3.2. Nonfluorinated Surfactant Systems. To understand the difference in the properties of RM containing surfactants with perfluorinated chains and nonfluorinated chains, we simulated a series of aqueous reverse micelles composed of nonfluorinated $PECOO^-NH_4^+$ surfactants in $scCO_2$. Because we are not aware of any experimental information about microemulsions created in systems with the hydrogenated analogue of PFPE, we were not able to use experimental information to set up the system. Therefore, the first system we simulated in the series (system 2) contained 554 water molecules, the same number of water molecules as in system 1. Starting from an aggregated configuration, we equilibrated system 2 for 500 ps followed by a 5 ns production run. We observed a distinct difference that existed between system 2 and the fluorinated surfactant system: the reverse micelle in system 2 had a much larger exposed aqueous core area. To obtain a quantitative estimate of the aqueous core exposure area in system 2, we again used the method of Lee and Richards[33] as described above. The exposed aqueous core area for the nonfluorinated system was found to be 32% compared to 12% in the case of the fluorinated system. As a result, a larger contact between CO_2 and water molecules is established in system 2. The large exposed core area has a form of patches that can be clearly seen in Figure 14. Why do we get these patches? As we shall see below, the hydrogenated tails of surfactant molecules experience stronger attraction between themselves than tails of fluorinated surfactants. Also, the hydrogenated surfactant is smaller in size, and therefore, in an assembly of hydrogenated surfactants, the area covered by headgroups must be smaller. If the number of water molecules inside the micellar pool is fixed, one ends up with regions where direct contact is established between water and carbon dioxide. In the experimental situation, water in the interior of the micelle will be exchanged with the exterior until the micelle acquires its minimum free energy. Because we use a canonical ensemble that fixes the number and type of molecules in the system and the length of our simulations is orders of magnitude shorter than the one needed to observe the major restructuring of the micellar system, we need to look for another strategy to perform a reasonable comparison of systems containing micelles with fluorinated or hydrogenated tails.

Therefore, for a comparison study we decided to find a system containing a reverse micelle with a hydrogenated analogue of PFPE that had the same exposed aqueous core area as system 1. For this purpose we carried out a few more simulations keeping the number of nonfluorinated surfactants fixed, but changing the number of water molecules. These systems with different water contents were then simulated for a long enough time to follow the extent of the exposed aqueous core area. We kept our search on until we picked up a system containing 200 water molecules. Our analysis showed that in this case an exposed aqueous core area (13%) was very similar to that found in the fluorinated surfactant system (system 1). This particular system (system 3) was simulated further for a production run of 5 ns to be able to compare the results from this simulation with the results from the simulation performed on the fluorinated surfactant system.

From the outset we want to point out an interesting fact about the systems containing a smaller amount of water. In their initial configuration they had a large contact between CO_2 and water. This was not just because our starting configuration was system 2 but also due to the fact that we had taken out quite a few water molecules randomly. However, as the simulation progressed, the surfactant molecules adjusted themselves to cover the aqueous core as homogeneously as they could, leaving small patches of aqueous core exposed to CO_2 here and there.

We calculated R_g for the aqueous core in system 3 by using the same formula as the one presented in eq 6. Again the contributions from water molecules in the core, NH_4^+ counterions, the carboxylate group, the adjacent CH_2 group, and the first ether oxygen (O3) in each of the surfactant tails were included in the calculation. We noticed a stable aggregated core during the 5 ns production run with an average value of R_c equal to 14.8 ± 0.3 Å. The calculated R_c values imply that the $PFPECOO^-NH_4^+$ surfactant will form a larger micelle compared to the model nonfluorinated $PECOO^-NH_4^+$ surfactant when the aqueous core exposure is the same. This is consistent with the smaller amount of water molecules in the aqueous pool of the nonfluorinated micelle. We also noticed that fluctuations in R_c are smaller for the nonfluorinated surfactant system compared to those observed in fluorinated surfactant system. A stronger packing (or attraction) between the hydrophobic tails of nonfluorinated surfactants may explain this observation. We will discuss this point in more detail later.

The stability of the aggregate was further tested by examining the time evolution of its eccentricity e. We found that the value of the eccentricity was stable in time confirming our observation about the stability of the micelle in system 3. The eccentricity for the system was found to fluctuate around the average value of 0.06. This value indicates that the aggregate in system 3 is quite spherical.

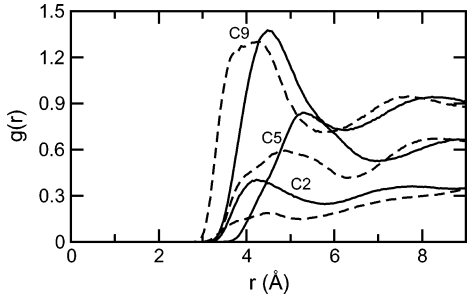

Figure 15. Radial distribution functions between carbon dioxide carbon and the C atoms along the surfactant backbone. Solid lines represent the fluorinated surfactant atoms, and dashed lines represent the nonfluorinated surfactant atoms in system 3. Atom notations are the same as shown in Figure 1.

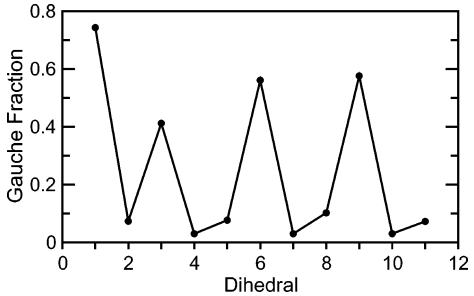

Figure 16. Average fraction of gauche defects for each dihedral angle present in the nonfluorinated surfactant in system 3. The dihedral angles are numbered in the same way as shown in Figure 8.

We calculated the area per headgroup for the model surfactant in system 3 by using both methods mentioned earlier. By using the method of Lee and Richards,[33] the obtained value is 35.1 ± 4 Å^2. The corresponding value from eq 8 is 41.7 Å^2. As we can see, the data show that the area available per $PFPECOO^-NH_4^+$ surfactant is larger than the area per nonfluorinated $PECOO^-NH_4^+$ surfactant. It is known that in microemulsions the area occupied by the surfactant molecule at the interface depends on the extent to which solvent molecules penetrate the hydrophobic tail region.[34]

Experimental studies indicate that surfactants with fluoroalkyl or fluoroether tails exhibit higher solubilities in CO_2 compared to surfactants with alkyl tails. Therefore, fluorinated surfactants form more stable W/C microemulsions.[1,7,35] We can use the results from our molecular dynamics simulation to get microscopic information concerning this issue. In Figure 15, we compare the rdf's of fluorinated surfactants with those of the nonfluorinated surfactants. For clarity, we compare only g_{Cc-C9}, g_{Cc-C5}, and g_{Cc-C2}. C9, C5, and C2 represent, respectively, the last, the middle, and the first carbon atoms along the backbone of the surfactant tail. The sharper and narrower first peaks indicate that the solvent coordinates more strongly to the fluorinated chains than to the nonfluorinated chains. In the fluorinated surfactant case, the first maximum of g_{Cc-C9} is at 4.5 Å whereas it is at 4.1 Å for the nonfluorinated surfactant. This shift is due to the smaller size of hydrogen compared to fluorine. The same holds for other rdfs. We also determined the average solvation number for nonfluorinated surfactants by counting the number of CO_2 molecules in the first solvation shell. The average value of the solvation number we obtained for system 3 is 10. This should be compared to 15 obtained for the fluorinated surfactant. Thus, we observe about a 33% lower solubility for the polyether surfactant compared to its fluorinated analogue. It is worth mentioning that the solvation number for the nonfluorinated surfactants in system 2 was also calculated to be 10. This is an indication that although the aqueous core in system 2 had a larger exposure to CO_2, the surfactant tails in systems 2 and 3 had the same exposure to molecules of CO_2. Using the method of Lee and Richards[33] again, we calculated the exposed aqueous core area in system 3. The average value of the accessible surface area we obtained for the bare aqueous core is 5450 ± 200 Å^2. An area of 709 ± 90 Å^2 is obtained when the surfactants were present in the system. Thus about 13% of the aqueous core was exposed to CO_2, which is comparable to the 12% in the case of the fluorinated surfactant system.

At this point we will attempt to answer the question why the perfluoropolyether chains are more soluble in CO_2 compared to their nonfluorinated analogues. One of the proposed reasons is that the dispersion force acting between the fluorinated chains matches well with that of the chain$-CO_2$ interaction.[47] Another important factor to be considered is the surfactant intertail interaction. A weaker tail$-$tail attraction will leave a wider space for CO_2 to penetrate the tail region and therefore will increase the solubility of the surfactants. On the other hand, a stronger intertail attraction will leave less room for CO_2 to penetrate between the tails and therefore will reduce the solubility. We calculated that the configurational energy for a pair of polyether surfactants is -1361 kJ/mol, whereas it is -342 kJ/mol for a pair of perfluoropolyether surfactants. The stabilization observed for the nonfluorinated surfactant pairs is due to the attraction between negatively charged ether oxygens and positively charged hydrogens on the adjacent tails. As a result of this stabilization the adjacent tails move closer in the case of nonfluorinated surfactants. No such specific interaction is present in the case of fluorinated surfactants. Thus, both the well-matched dispersion force acting between the surfactant tail and CO_2 molecules and wider intertail space help fluorinated chains to accumulate more CO_2 around them. As we already mentioned, the large intertail attraction experienced between tails of polyether surfactants is also responsible for the observed exposure of water to CO_2 in system 2.

We also considered the change in tail conformations when we replaced fluorine atoms with hydrogens. Figure 16 depicts the average fraction of gauche defects for each dihedral angle present in the nonfluorinated surfactant from system 3. The numbering and the calculation procedure are similar to the one adopted for system 1. We observed a very similar distribution of gauche defects in systems 1 and 3, except that in system 3 the fraction of gauche angles is somewhat larger. This is due to the presence of smaller and lighter hydrogens in the nonfluorinated tails.

4. Summary and Conclusions

Molecular dynamics simulations provide a powerful tool to gain detailed molecular information about structural and dynamical properties of reverse micelles that is otherwise very difficult, even sometimes impossible, to get by means of experiments or using analytical theoretical techniques. In this paper we report results obtained from simulations on reverse micelles created in a ternary system: surfactant/water/supercritical carbon dioxide. In the simulation with the PFPE surfactant we used experimental data to determine the number of particles in the system. For this system we observed a stable spherically shaped micelle that displayed geometrical properties in pretty good agreement with experiments. When we replaced fluorine atoms in the surfactant molecules with hydrogen atoms and preserved the value of W_o, we observed a strong increase in the direct contact between water and CO_2. This should result

in an increase of the system free energy and therefore destabilize the micelle, thus providing support to the idea that fluorinated surfactant molecules are helpful for the production of microemulsions in water/carbon dioxide systems. To compare micelles with fluorinated and hydrogenated surfactants, we decided to look at a system that had the same exposed aqueous core to CO_2. In this case we found that the micelle with hydrogenated surfactants had a smaller value of W_o. We also found that the micelle containing surfactant molecules with fluorinated tails is better solvated in CO_2. This explains why fluorinated surfactants are preferred for technical applications.

In our simulations we observed regions of broad interfaces, but we also observed that both water and CO_2 reach bulk density values at distances that are a few molecular diameters away from the interface. We saw that most of the ammonium counterions are situated next to the charged headgroups of the surfactants, thus creating ion pairs. It will be very interesting to study what effect the nature of the counterions has on the structure of the micelle and this will be the subject of our next investigation.[46]

Acknowledgment. This work was supported by the Kenan Center for the Utilization of Carbon Dioxide in Manufacturing and the STC Program of the National Science Foundation under Agreement CHE-9876674. The simulations were performed on an IBM SP machine at the North Carolina Supercomputing Center. We thank Lanyuan Lu for helping us in building the starting configuration and for many helpful discussions. Conversations with Professor Keith P. Johnston were very useful. S.S. thankfully acknowledges Kenneth M. Lee for providing the site charges on the $PECOO^-$ surfactant anion.

References and Notes

(1) Consani, K. A.; Smith, R. D. *J. Supercrit. Fluids* **1990**, *3*, 51.
(2) Harrison, K.; Goveas, J.; Johnston, K. P.; O'Rear, E. A. *Langmuir* **1994**, *10*, 3536.
(3) Johnston, K. P.; Harrison, K. L.; Clarke, M. J.; Howdle, S. M.; Heitz, M. P.; Bright, F. V.; Carlier, C.; Randolph, T. W. *Science* **1996**, *271*, 624.
(4) DeSimone, J. M.; Maury, E. E.; Menceloglu, Y. Z.; McClain, J. B.; Romack, T. J.; Combes, J. R. *Science* **1994**, *265*, 356. DeSimone, J. M.; Guan, Z.; Elsbernd, C. S. *Science* **1991**, *257*, 945.
(5) Keiper, J. S.; Simhan, R.; DeSimone, J. M.; Melnichenko, Y. B.; Wignall, G. D.; Frielinghaus, H. *J. Am. Chem. Soc.* **2002**, *124*, 1834.
(6) Steytler, D. C.; Rumsey, E.; Thorpe, M.; Eastoe, J.; Paul, A.; Heenan, R. K. *Langmuir* **2001**, *17*, 7948.
(7) Hoefling, T. A.; Enick, R. M.; Beckman, E. J. *J. Phys. Chem.* **1991**, *95*, 7127. Beckman, E. J. *Science* **1996**, *271*, 613−614.
(8) Eastoe, J.; Cazalles, B. M. H.; Steytler, D. C.; Holmes, J. D.; Pitt, A. R.; Wear, T. J.; Heenan, R. K. *Langmuir* **1997**, *13*, 6980.
(9) Eastoe, J.; Bayazit, Z.; Martel, S.; Steytler, D. C.; Heenan, R. K. *Langmuir* **1996**, *12*, 1423.
(10) Lee, C. T.; Johnston, K. P.; Dai, H. J.; Cochran, H. D.; Melnichenko, Y. B.; Wignall, G. D. *J. Phys. Chem. B* **2000**, *104*, 11094.
(11) Lee, C. T.; Johnston, K. P.; Dai, H. J.; Cochran, H. D.; Melnichenko, Y. B.; Wignall, G. D. *J. Phys. Chem. B* **2001**, *105*, 3540.
(12) Zielinski, R. G.; Kline, S. R.; Kaler, E. W.; Rosov, N. *Langmuir* **1997**, *13*, 3934.
(13) Senapati, S.; Keiper, J. S.; DeSimone, J. M.; Wignall, G. D.; Melnichenko, Y. B.; Frielinghaus, H.; Berkowitz, M. L. *Langmuir* **2002**, *18*, 7371.
(14) Clarke, M. J.; Harrison, K. L.; Johnston, K. P.; Howdle, S. M. *J. Am. Chem. Soc.* **1997**, *119*, 6399.
(15) Assih, I.; Larche, F.; DeLord, P. *J. Colloid Interface Sci.* **1982**, *89*, 35.
(16) Pileni, M.-P.; Zemb, T.; Petit, C. *Chem. Phys. Lett.* **1985**, *118*, 414.
(17) Senapati, S.; Berkowitz, M. L. *J. Chem. Phys.* **2003**, *118*, 1937.
(18) Salaniwal, S.; Cui, S. T.; Cochran, H. D.; Cummings, P. T. *Langmuir* **1999**, *15*, 5188.
(19) Salaniwal, S.; Cui, S. T.; Cochran, H. D.; Cummings, P. T. *Ind. Eng. Chem. Res.* **2000**, *39*, 4543; *Langmuir* **2001**, *17*, 1773.
(20) Berendsen, H. J. C.; Grigera, J. R.; Straatsma, T. P. *J. Phys. Chem.* **1987**, *91*, 6269.
(21) Dauber-Osguthorpe, P.; Roberts, V. A.; Osguthorpe, Wolff, J.; D. J.; Genest, M.; Hagler, A. T. *Proteins: Struct. Funct. Genet.* **1988**, *4*, 31.
(22) *Discover User Guide Part I*; Biosym Technologies, CA, 1993.
(23) Koike, A. *J. Phys. Chem. B* **1999**, *103*, 4578. Koike, A.; Yoneya, M. *J. Chem. Phys.* **1996**, *105*, 6060.
(24) da Rocha, S. R. P.; Johnston, K. P.; Rossky, P. J. *J. Phys. Chem. B* **2002**, *106*, 13250.
(25) Jorgensen, W. L.; Gao, J. *J. Phys. Chem.* **1986**, *90*, 2174.
(26) Harris, J.; Yung, K. H. *J. Phys. Chem.* **1995**, *99*, 12021.
(27) Cicotti, G.; Ryckaert, J. P. *Comput. Phys. Rep.* **1986**, *4*, 345.
(28) Fincham, D. *Mol. Simul*. **1992**, *8*, 165.
(29) Nagashima, K.; Lee, C. T.; Xu, B.; Johnston, K. P.; DeSimone, J. M.; Johnson, C. S., Jr. *J. Phys. Chem. B* **2003**, *107*, 1962.
(30) Nose, S. *J. Chem. Phys*. **1984**, *81*, 511. Hoover, W. G. *Phys. Rev. A* **1985**, *31*, 1695.
(31) Essmann, U.; Perera, L.; Berkowitz, M. L.; Darden, T.; Lee, H.; Pedersen, L. G. *J. Chem. Phys.* **1995**, *103*, 8577.
(32) Smith, W.; Forester, T. R. DLPOLY, 2.12 version. CCLRC, Daresbury Laboratory, 1999.
(33) Lee, B.; Richards, F. M. *J. Mol. Biol.* **1971**, *55*, 379.
(34) Mukherjee, S.; Miller, C. A.; Fort, T. J. *J. Colloid Interface Sci.* **1983**, *91*, 223.
(35) Lezzi, A.; Bendale, P.; Enick, R. M.; Turberg, M.; Brady, *J. Fluid Phase Equilib.* **1989**, *52*, 307.
(36) Tobias, D. J.; Klein, M. L. *J. Phys. Chem.* **1996**, *100*, 6637.
(37) Jorgensen, W. L.; Binning, R. C.; Bigot, B. *J. Am. Chem. Soc.* **1981**, *103*, 4393.
(38) Scarsi, M.; Apostolakis, J.; Caflisch, A. *J. Phys. Chem. B* **1998**, *102*, 3637.
(39) Tanabe, K. *Spectrochim. Acta, Part A* **1972**, *28A*, 407.
(40) Senapati, S.; Chandra, A. *J. Chem. Phys.* **1999**, *111*, 1223.
(41) Levinger, N. E. *Curr. Opin. Colloid Interface Sci.* **2000**, *5*, 118. Riter, R. E.; Undiks, E. P.; Levinger, N. E. *J. Am. Chem. Soc.* **1998**, *120*, 6062.
(42) Willard, D. M.; Riter, R. E.; Levinger, N. E. *J. Am. Chem. Soc.* **1998**, *120*, 4151. Riter, R. E.; Willard, D. M.; Levinger, N. E. *J. Phys. Chem. B* **1998**, *102*, 2705.
(43) Datta, A.; Mandal, D.; Pal, S. K.; Bhattacharyya, K. *J. Phys. Chem. B* **1997**, *101*, 10221. Das, S.; Datta, A.; Bhattacharyya, K. *J. Phys. Chem. A* **1997**, *101*, 3299.
(44) Faeder, J.; Ladanyi, B. M. *J. Phys. Chem. B* **2001**, *105*, 11148; *J. Phys. Chem. B* **2000**, *104*, 1033.
(45) Balasubramanian, S.; Bagchi, B. *J. Phys. Chem. B* **2002**, *106*, 3668. Pal, S.; Balasubramanian, S.; Bagchi, B. *J. Chem. Phys.* **2002**, *117*, 2852.
(46) Senapati, S.; Berkowitz, M. L. Manuscript in preparation.
(47) O'Neill, M. L.; Cao, Q.; Fang, M.; Johnston, K. P.; Wilkinson, S. P.; Smith, C. D.; Kerschner, J. L.; Jureller, S. H. *Ind. Eng. Chem. Res.* **1998**, *37*, 3067.